

Design, Analysis, and Testing of the Prox-1 Satellite Structure

Thomas D. Pappas

Prox-1 Structural Subsystem Team Lead
tpappas3@gatech.edu

David A. Spencer

Research Advisor, Prox-1 Principal Investigator
david.spencer@aerospace.gatech.edu

Institute: Georgia Institute of Technology
Department: Daniel Guggenheim School of Aerospace Engineering
Laboratory: Center for Space Systems
Course: AE 8900, Special Problem Course

Table of Contents

Nomenclature	3
Acknowledgements	4
I. Introduction.....	5
II. Subsystem Requirements.....	6
III. Design	9
A. R3: Lessons Learned.....	9
B. Key Structural Features.....	10
C. Initial Packing	12
D. Redesigned Structure and Packing	13
IV. Testing	15
A. Fabrication of the Test Structure.....	15
B. Interface Plate Design and Fabrication.....	16
C. Shake Table Setup.....	17
D. Testing Procedure and Results	19
V. Finite Element Analysis.....	24
A. Test Structure Model and Analysis	24
B. Packing Structure Model and Analysis.....	25
VI. Conclusion.....	29
Appendix A. Images of Vibrational Modes from Analysis.....	30
1. Test Structure.....	30
2. Redesigned Structure	33
3. Redesigned Structure with Packing	36
Appendix B. Part Drawings for the Test Structure and Interface	39

NOMENCLATURE

CAD – Computer Aided Design

FEA – Finite Element Analysis

LVI – Launch Vehicle Interface

NUG – Nanosat User’s Guide

Prox-1 – Proximity Operations satellite for UNP-7

R3 – Rapid Reconnaissance and Response satellite for UNP-6

UNP – University Nanosat Program

ACKNOWLEDGEMENTS

There are several people without whom this product would not have been possible and that I would like to thank. First and foremost, Prof David Spencer who gave me the privilege of working on the R3 and Prox-1 satellite design projects. As my research advisor and the principal investigator of Prox-1, his advice and prior experience has been indispensable to my continued learning throughout my graduate career. Also, I would like to thank Dr. Massimo Ruzzene who graciously gave me access to use his structural testing lab and equipment as well as his graduate student, Filippo Casadei, who took time out of his undoubtedly busy schedule to help me with the structural testing. A special thanks to Scott Elliot and Scott Moseley for giving me open access to their machine shop and helping me to machine the test structure. Their wealth of knowledge has taught me over the years how to design for machinability. Finally, a thanks to the entire Prox-1 team for making Prox-1 a great project to work on.

I. INTRODUCTION

Detailed design of the Prox-1 satellite began in January 2011 as a submission for the University Nanosat Program -7 competition administered by the AFRL. The mission will see Prox-1 deploy a cubesat from an integrated PPOD and track it using a visible and infrared camera. Based on estimated attitude and range data derived from image processing, Prox-1 will use artificial potential functions to autonomously conduct a low thrust rendezvous with cubesat and then proceed into a series of proximity operations.

Leveraging past experience with the R3 satellite project (submitted for UNP-6), a completely new structure was designed for Prox-1 to not only meet the UNP requirements but also be easier, faster, and more reliable to fabricate. From a smaller overall size and thicker plates to designing with the specific capabilities and limitations of computerized machining in mind, the Prox-1 structure proved a substantial improvement over R3. Key design choices for various structural features are detailed and their rationale explained. Physical testing of a machined prototype structure as well as finite element analysis of a number of computer models prove the structure meets UNP requirements.

II. SUBSYSTEM REQUIREMENTS

The requirements for the structural subsystem are mostly taken from the Nanosat User’s Guide (NUG). Additional requirements are derived from the needs of specific components in other subsystems. As a whole, the structural requirements don’t flow down from the mission success criteria in the way that the requirements for other subsystems do. Higher level system requirements are therefore not included here.

The NUG requirements mostly focus on ensuring the safety and survivability of the system. These act as a guideline for students that most likely have never designed a satellite in such detail before by giving boundaries and pointing in the right direction. They also serve to ensure the safety of the primary launch payload from damage. As a result, the requirements given by the NUG are somewhat stricter than would be expected for a satellite.

Of particular note are the loading and vibration requirements. These will be the focus of this paper. The loading requirement states that the satellite must sustain 20 Gs of acceleration along each axis. The vibration requirement states that no vibrational modes can have a natural frequency below 100 Hz. Of the two, the vibration requirement is much stricter and typically if it can be met then the loading requirement is also met.

Table 2.1. Structural Subsystem Requirements

Index	Requirement	Source
STR-1	The integrated Prox-1 system shall be designed to withstand the launch vehicle shock and vibroacoustic environment without failure.	NUG
STR-2	The Prox-1 satellite shall be capable of withstanding an acceleration load factor that correspond to worst-case launch load environments, which is a combination of steady-state, low-frequency, transient loads and high-frequency vibration loads. This design limit load factor is ± 20.0 g's on each axis, applied through the center of mass of the analyzed component using the NS-6 coordinate system.	NUG
STR-3	Fracture control shall be implemented according to NASA-STD-5003, including multiple load paths and structures built with machined (milled) metals with well-understood properties and having low stresses.	NUG

STR-4	Multiple locking threaded fasteners with backout protection shall be used to join components and assemblies for fastener redundancy and hazard protection.	NUG
STR-5	As required by JSC 23642, all primary bus structure fasteners shall be #10 or larger and all electronics enclosures shall be fastened to the structure using #8 or larger fasteners.	NUG
STR-6	Prox-1 shall have a fixed base natural frequency (at the SIP) of >100Hz.	NUG
STR-7	The center of gravity (CG) for the Prox-1 satellite shall be less than 0.5 cm from the Lightband centerline, including manufacturing tolerances.	NUG
STR-8	The center of gravity (CG) for the Prox-1 satellite shall be less than 40 cm above the SIP (+Z axis).	NUG
STR-9	All components shall have adequate venting as defined in Section 6.3.3.6 of the Nanosat-6 User's Guide. The Prox-1 satellite shall not have pressure vessels or sealed compartments. Venting analysis shall demonstrate a factor of safety of 2.0.	NUG
STR-10	The integrated Prox-1 satellite shall be designed to withstand the AFRL Sine Burst Test at 1.2 times the limit loads and a frequency of 0.33 times the lowest natural frequency with no detrimental permanent deformation or ultimate failures.	NUG
STR-11	The structure of the Prox-1 satellite shall conform where applicable to the requirements of NSTS 1700-7B.208 and NASA-STD-5003 excepting where specific requirements are defined by the NUG.	NUG
STR-12	Structural Safety Factors shall meet or exceed 2.0 for yield and 2.6 for ultimate unless otherwise specified by the NUG or other documents listed above.	NUG
STR-13	Mechanism Load Safety Factors for both operating torque margin and holding torque margin shall meet or exceed 1.0 if based on test and 2.0 if based on analysis.	NUG
STR-14	The Prox-1 satellite shall have a local flatness of 0.0005 inches per inch at the SIP.	NUG
STR-15	The primary structure of the Prox-1 satellite shall be machined (milled) and all-metallic.	NUG
STR-16	Pyrotechnic devices/mechanisms shall not be used on the Prox-1 satellite.	NUG

STR-17	The Prox-1 satellite shall not use welded joints or cast metallic components.	NUG
STR-18	A margin of safety (MS) of zero or greater shall exist for both yield and ultimate stress conditions.	NUG
STR-19	Bolts used in flight hardware shall be lubricated with space-rated lubricant and torqued to values specified in Table X of MSFC-STD-486B.	NUG
STR-20	Retaining devices that rely solely on friction as a means of retention (such as, but not limited to: crimps, worm gears, lead screws, and motor detent torques) shall not be used.	NUG
STR-21	The Prox-1 satellite shall accommodate the mounting, placement, and structural support needs of all components of engineering subsystems.	SS-2
STR-21.1	The Prox-1 satellite shall provide a stable mounting platform for optical instruments on the nadir-pointing face.	STR-21
STR-21.1.1	Structural deformation shall not permanently compromise the alignment or operation of optical instruments.	STR-21.1
STR-21.2	The Prox-1 satellite shall interface with a 3u PPOD and provide for an uninhibited deployment of the Cubesat.	STR-21

III. DESIGN

R3: Lessons Learned

For the University Nanosat Program (UNP) – 6 competition, Georgia Tech submitted the R3 satellite. The UNP-6 cycle began in January, 2009 and ended in January, 2011. I worked as the structural team lead for the latter half of the cycle and learned quite a bit from the design and fabrication of R3's structure that informed the design of Prox-1.

R3's power requirements as well as the decision to use body-mounted solar arrays necessitated a relatively large structure. The final dimensions measured 46x46x52 cm and pushed right up against the UNP sizing limits. To create a structure this large while at the same time limiting the structural mass required the use of rather thin exterior plates (3/16" thick aluminum) and sparing internal structural support. With a large unconstrained interior on such a relatively thin plate, each plate featured a number of low frequency vibrational modes. While attaching the various satellite components to the exterior plates helped to constrain the interior region of the plates, the additional mass ultimately lowered the frequencies even more.

Such thin plates could not support bolting directly to each other so brackets were placed in the center of each edge to attach neighboring plates. While these were able to carry the necessary loads just fine, they left long edges along the corners of the plates unconstrained. The plate edges were therefore left to vibrate in a flapping motion.

Satellites in the UNP competition are required to use the Lightband launch vehicle interface (LVI) which is essentially a 15" diameter spring-loaded ring with electronic latches. When the latches are released, the springs push the satellite away from the launch vehicle. The size of the R3 satellite allowed it to hang over the lightband by several inches on each side. Combined with its high center of gravity and thin bottom plate the entire satellite would rock back and forth on the LVI like a pendulum at very low frequencies.

Finally, machining the structure proved very difficult. The thin sheets of aluminum were prone to deforming while machining and due to the tolerances of my own inexperience many cuts had to be remade and many bolt holes had to be widen or drilled again. While these imperfections never compromised the structure, they did decrease its rigidity which again lowered the natural frequencies.

Leaving R3 and starting fresh with Prox-1, it was imperative to deal with the core issues of R3 that caused it to fail to meet its requirements. Five design goals were set to accomplish this.

1. Prox-1 should be made as small as possible. Not only would reducing the plate sizes automatically increase the natural frequencies at which they vibrated but the mass saved could

be used to make the plates thicker and more rigid. Ideally, two of Prox-1's dimensions should be limited to the size of the Lightband interface to completely eliminate the possibility of a rocking vibrational mode.

2. Prox-1 should use thicker plates. A thickness of 3/16" was sufficiently capable of supporting the required loading but simply was not rigid enough to meet the frequency requirement. Ideally, the plates should be thick enough to allow the plates to bolt directly to each other rather than through a bracket or similar interface.

3. The exterior plates must be constrained to each other as much as possible. This includes constraints along each edge and in the interior of the plates if possible. The less that the plates are given the freedom to vibrate, the higher their natural frequencies will be.

4. Cut as much structural mass as possible. R3's plates had relatively few cutouts because of the number of components that needed to attach to them. Much of this mass could be removed without impacting the stiffness of the plate to nearly the same degree. This increases the stiffness to mass ratio of the plate and therefore its natural frequencies.

5. Use computerized machining processes as much as possible. The level of precision these allow will significantly improve build quality. Unfortunately, they are somewhat limited in their capabilities and these limitations need to be accounted for and accommodated into the structural design.

Key Structural Features

A number of key structural features were chosen very early in the design process to ensure that Prox-1's structure met the UNP's vibration requirements. The overall dimensions of the structure were set to 16x16x8 inches. This represented a significant decrease in size relative to R3. The 16" square base placed the satellite exactly within the footprint of the LVI while the 8" height lowered the center of gravity tremendously.

The six exterior plates featured significant cutouts to remove as much mass as possible. Shown in Figure 3.1, the edges of each plate were 1/2" thick as the primary load bearing and stiffening members of the structure while the interior webbing of the plates was 1/4" thick to save mass. Such thick edges allowed plenty of room for 1/4"-20 bolts to pass through the face of one plate and into the side of the neighboring plate. Two of these bolts were used to attach each plate to each other plate in the corners while interlocking teeth helped to constrain the rest of each edge. The bolt heads were countersunk into each plate to avoid collision with the eventual solar panels. Figure 3.2 shows a close-up of this technique along one edge. Despite the substantial

increase in plate thickness, the smaller size and aggressive cutouts reduced the mass of each by about half to ~0.6kg relative to the R3 plates.



Figure 3.1. 3D CAD model of a side plate.

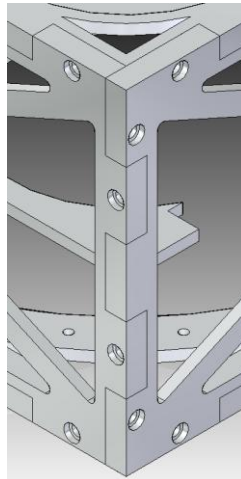


Figure 3.2. Close-up of interlocking plate edges.

A horizontal shelf was placed midway up the height and spanned the interior of the structure. This served as the main mounting point for the majority of the satellite components. It attached in the center of each side plate (helping to further constrain those plates) as well as in the corners of the structure. Figure 3.3 shows the complete structure modeled in the 3D CAD Solid Edge.

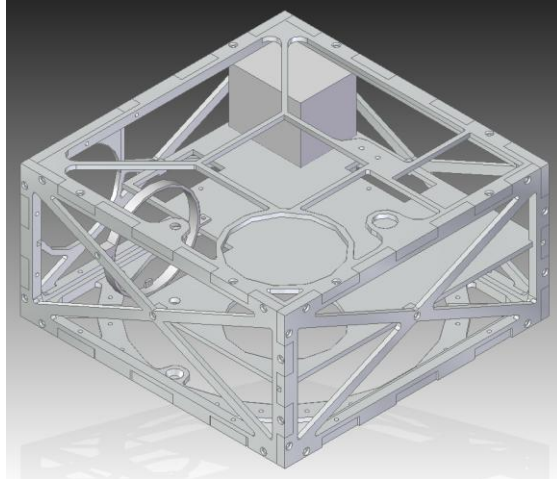


Figure 3.3. 3D CAD model of the assembled structure.

Throughout the design of the various plates, an effort was made to keep them as two-dimensional as possible. This means that most of the features can be cut directly into the face of the plate and most of these pass entirely through the plate. Similarly, no features stick out from the plate. This is to facilitate a simpler fabrication process with much fewer steps. Automated machines such as the waterjet cutter and CNC can only work in two dimensions and as previously stated in the design goals, it's desirable to have these sorts of machines do as much of the actual machining as possible. The only major features that do not follow these rules are the holes drilled into the plate sides. These unfortunately needed to be drilled by hand as one of the final steps in fabrication.

Initial Packing

Any packing begins with those components that have the most stringent requirements. In the case of Prox-1, those components were the ion thruster and the PPOD. The ion thruster would exert a force on the satellite and even though that force was very small it would be sustained for long periods of time with the potential to induce a rather large integrated moment. By placing the ion thruster in the center of the satellite along the z axis, this could easily be avoided. Deploying the 4kg cubesat from the satellite would cause a small but significant shift in the center of mass of the satellite. This shift could cause unnecessary complexity by requiring mid-mission adjustments to things like attitude control laws so it was desirable to limit the movement of the center of mass to be along as few axes as possible. This consideration was most important with respect to the ion thruster and therefore the PPOD was also mounted along the z axis.

The visible and infrared cameras were placed facing out the top of the satellite similar to the PPOD so that they could acquire and track the cubesat immediately upon deployment. They were positioned toward the corners of the satellite so that the overhanging PPOD did not obstruct their views before or after deployment of the cubesat when the PPOD's lid would swing open. Unfortunately, the overhanging PPOD did impinge on the star tracker and it was forced to face out one of the sides.

The UNP requires that the center of mass of the satellite be within 0.5cm of the centerline of the LVI. This implies that heavier components be distributed around the satellite evenly so as to counterbalance each other and keep the center of mass in the center of the satellite. The four heaviest components (battery box, IR camera, propellant tank, and star tracker) were each positioned in their own corner of the satellite. Similarly, a center of mass as close to the LVI was desired so heavier components were placed toward the bottom of the satellite where possible.

At this point, much of the internal mounting area was accounted for leaving the smaller, lighter components such as the communication equipment to be fit in between. Figure 3.4 shows a detail of the packing of the satellite with a number of callouts for the major components.

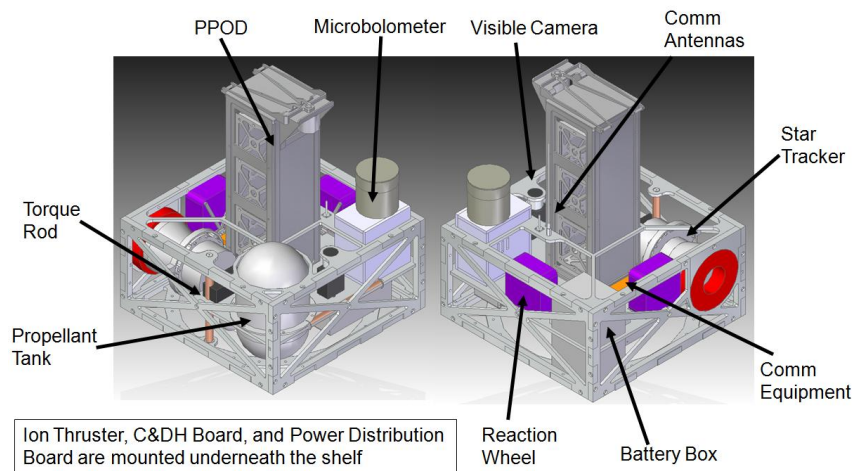


Figure 3.4. Packing model with callouts.

Redesigned Structure and Packing

Recently, a number of significant changes have been made to the core design of Prox-1. The ion thruster was replaced due to its complexity with two self-contained hot gas thrusters. These still provide the sustained low thrust necessary for mission success but in a much smaller and simpler package. The assumption of deployable solar arrays was discarded in favor of simpler body-mounted arrays. The star tracker was replaced by sun sensors. All of these changes motivated a complete rethink of the structure and packing of Prox-1. Allison Willingham has

done most of the work to update the structure and packing to accommodate these changes. It is presented here in overview as context for the analysis detailed later.

Many of the major components have been repositioned. The PPOD has been incorporated into the structure and now points out one of the sides. The two hot gas thrusters have been positioned to face out the center of two of the sides. It was determined that the cameras should face in line with one of the thrusters to minimize the amount of slewing that would be required between tracking the cubesat and conducting a burn. The large horizontal shelf has been replaced by two large vertical shelves to support the PPOD as well as a number of smaller supporting structures. The top and bottom plates have been converted to support the body mounted solar arrays. While the overall dimensions and features of the exterior plates have remained largely the same, the repositioning of all of the equipment has significantly changed the structure. Due to the shelf being removed in the new structure it was decided to also leave the shelf out of the test structure to try to maximize similarities.

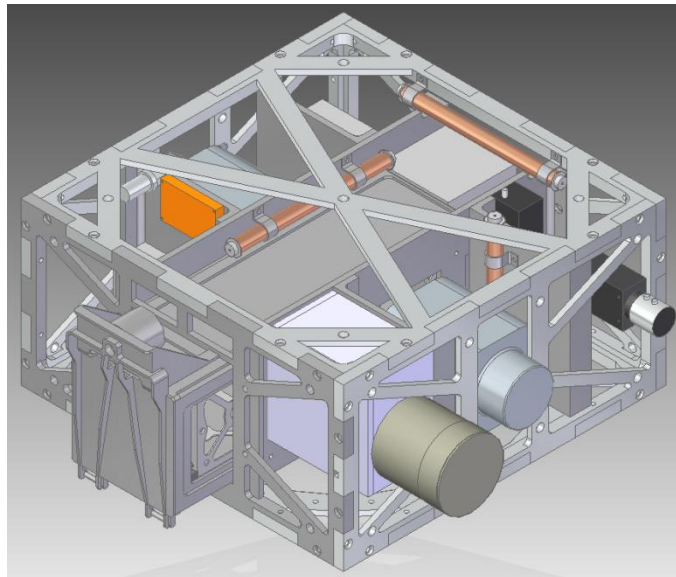


Figure 3.5. Redesigned packing model with callouts.

IV. TESTING

Fabrication of the Test Structure

Once the design of the structure had reached a fairly complete state, it was decided to proceed with the fabrication and testing of a prototype structure. Refer to Appendix B for the detailed drawings of the test structure plates. As stated previously, the plates were specifically designed so that most of the machining could be done with computerized equipment in an effort to reduce the variance of the interconnecting features.

The process began with several large 2ftx2ftx0.5in plates. The first step was to cut out the general outline of the plates using an abrasive waterjet. The waterjet injects garnet sand into a high-pressure stream of water to pierce and cut through up to six inches of steel. Cutting through a half inch of Aluminum by comparison would be quick and easy. It uses a 2D CAD file to determine its pathing and guide the cutting head precisely through curves and corners. Unlike the CNC machine which uses an actual end mill, the tiny diameter of the column of water used for cutting by the waterjet essentially allows it to cut internal angles. This feature necessitated its use for at least the outer edge of the plates. At that point the internal cutouts of the plates could be done using the CNC machine but the intense heat generated from extended milling to remove so much mass has the potential to warp softer materials like Aluminum. This again makes the waterjet the preferred machine for the large internal cutouts. Even the through holes in the face of the plates to accommodate the bolts were cut using the waterjet. Essentially, any feature that passed straight through the plate was cut using the waterjet.

Despite the usefulness of the waterjet, the CNC machine was still required. Its use of an end mill gives it the unique ability to remove material in successive layers from the face of a plate. This makes it ideal for thinning out the internal webbing of the plates from $\frac{1}{2}$ " to $\frac{1}{4}$ ". Similar to the waterjet, the CNC uses a 2D CAD file to generate its pathing and guide the bit around the various contours.

With most of the major features cut using the waterjet and the CNC, relatively little was left to do by hand. To ensure that the bolt holes lined up between plates, the two plates were held together while the drill bit was passed through the already cut hole of the first plate and into the side of the underlying plate. These holes were then tapped to accommodate the $\frac{1}{4}$ "-20 bolts. Countersinks for each bolt hole in the face of each plate were drilled using a specially designed bit so that the head of the bolts would sit flush with the face of the plate. Finally, some grinding over the plates allowed them to fit more easily with each other and removed sharp edges. Figure 4.1 shows one of the completed side plates.

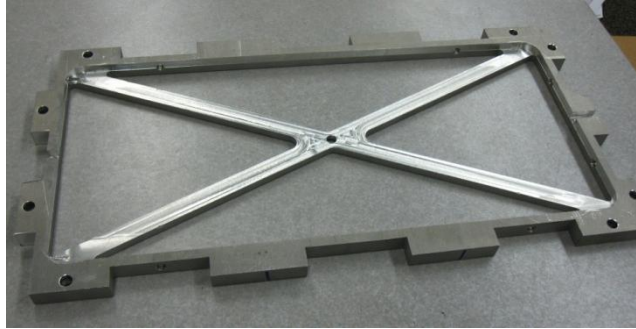


Figure 4.1. One of the completed side plates.

With all the plates completed, the structure was assembled without any trouble. All of the bolt holes lined up and all of the interlocking edges fit snugly. No adjustments were necessary. Figure 4.2 shows the fully assembled test structure.



Figure 4.2. The assembled test structure.

Interface Plate Design and Fabrication

An additional structure was determined to be necessary to interface between the shake table and the satellite structure. It was important for this structure to mimic the Lightband interface as closely as possible in its connection to the satellite while adapting to the fixed bolt pattern of the shake table. Two separate plates were needed to accomplish this. The first plate was cut to be a large 15" ring with dimensions and the 24 bolt hole pattern to match the Lightband. This plate was then mounted onto a separate rectangular base plate with bolt patterns for the Lightband ring and the shake table. This allowed the 24 Lightband bolts to pass up through the base plate and the Lightband ring and attach into the bottom plate of the structure. Once the structure was aligned on the shake table, another set of bolts could be passed down through the base plate and attached into the shake table. To ensure that the base plate sat evenly and

securely on the shake table, the bolt holes for the Lightband interface had to be countersunk into the base plate. Both plates were cut from 3/6" Aluminum 6061 because this was the thinnest they could be while still allowing enough room to accommodate the countersunk bolt heads. Reference Appendix A for the detailed drawings of these plates.

The waterjet was used to cut out the complex bolt patterns of both plates exactly while the countersunk holes were drilled by hand. Figure 4.3 shows the two interface plates separately and assembled and Figure 4.4 shows how the interface plate attaches to the structure.

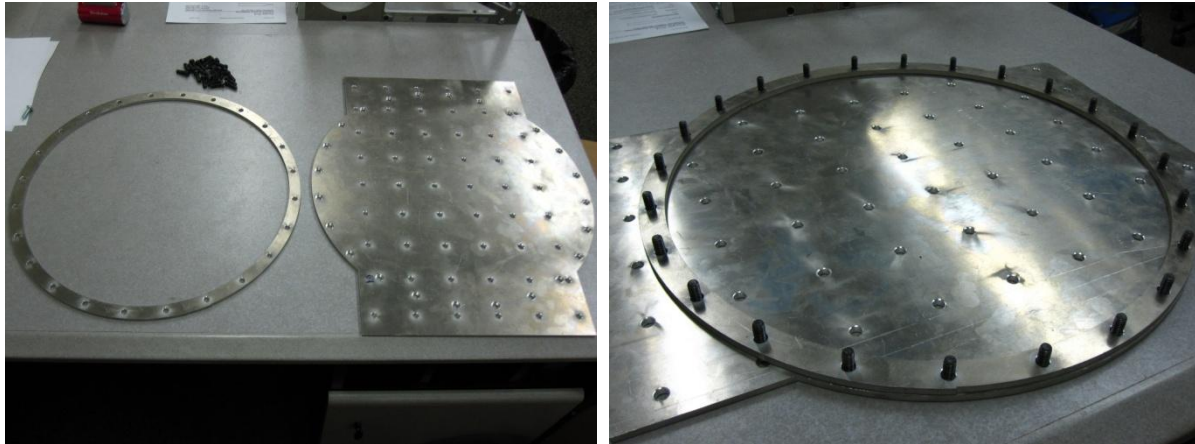


Figure 4.3. The shake table interface plates.

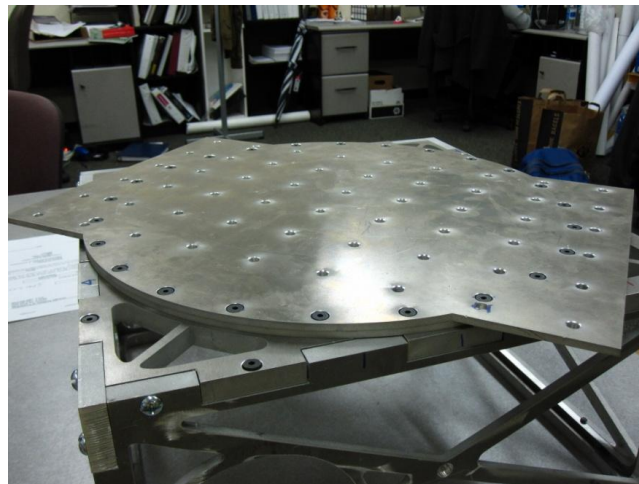


Figure 4.4. The shake table interface mounted to the test structure.

Shake Table Setup

Due to its relatively small size and weight, a small shake table was found to adequately excite the structure. The table itself featured a regular square pattern of attachment holes and was mounted on a set of linear bearings. This was then rigidly attached to a large motor which was

given its control signal by special software on a nearby computer. Unfortunately, this shake table was only able to excite the structure along a single axis at a time. The shake table is shown in Figure 4.5. The shake table interface was attached first to the satellite structure and then the entire structure was positioned and mounted to the shake table as shown in Figure 4.6 so that one of the side plates of the structure sat perpendicular to the line of excitation.

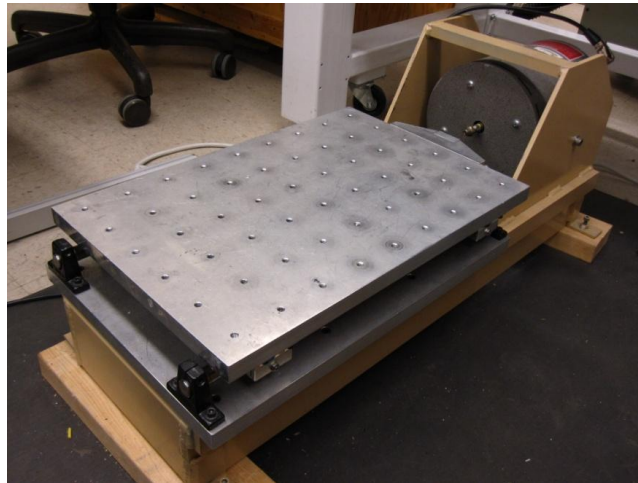


Figure 4.5. The shake table used for testing.

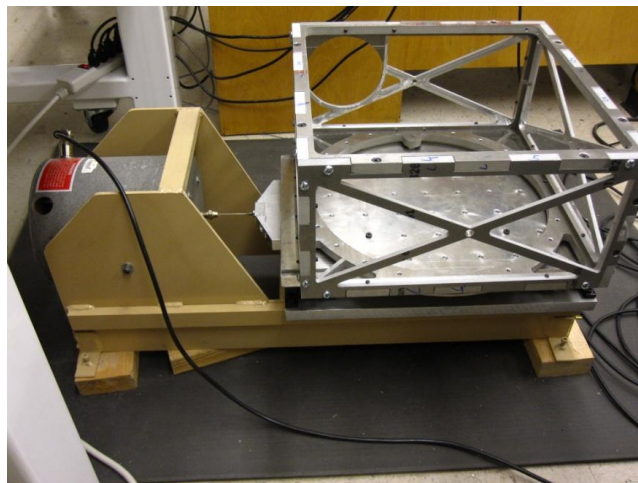


Figure 4.6. The test structure mounted to the shake table.

A few feet away, a laser was set up to face the structure perpendicularly. This laser, shown in Figure 4.7, measured the Doppler shift in its reflected beam to calculate the velocity of the structure at a specific point and transmitted this result back to the control computer for processing.



Figure 4.7. The laser instrument used for testing.

Test Procedure and Results

With the structure mounted securely to the shake table and the laser positioned for the first test, a software was used to set up the automated test procedure. A visible camera feed from the laser instrument was used to define points for data collection. A number of parameters for the control signal and the data processing were tweaked and refined throughout to try to get the best results possible in the desired frequency range. Figure 4.8 is a screenshot taken of the control software during one of the initial test runs. The top window shows the visible camera feed with a few test points defined while the window below shows the Fourier transform for one of the points being calculated in real time.



Figure 4.8. Screenshot of the testing software.

End to end, the software sends a pseudorandom control signal to the shake table motor. The laser measures the amplitude of vibration (velocity) of the structure at the defined point and

returns this signal to the software. The ratio of the measured and control signals is taken in the time domain (units of m/s/V) and this is used to calculate the Fourier transform. Averaging this result over a period of time (typically a few minutes) improves the coherence of the results. The user can then call out specific frequencies of interest and view the corresponding mode.

Two main data runs were conducted. The first took about ninety minutes and measured the vibration across one of the side plates. This test positioned the structure and laser as previously shown in Figures 4.6 and 4.7 respectively. The resulting averaged Fourier transform for the side plate is plotted in Figure 4.9 in dB.

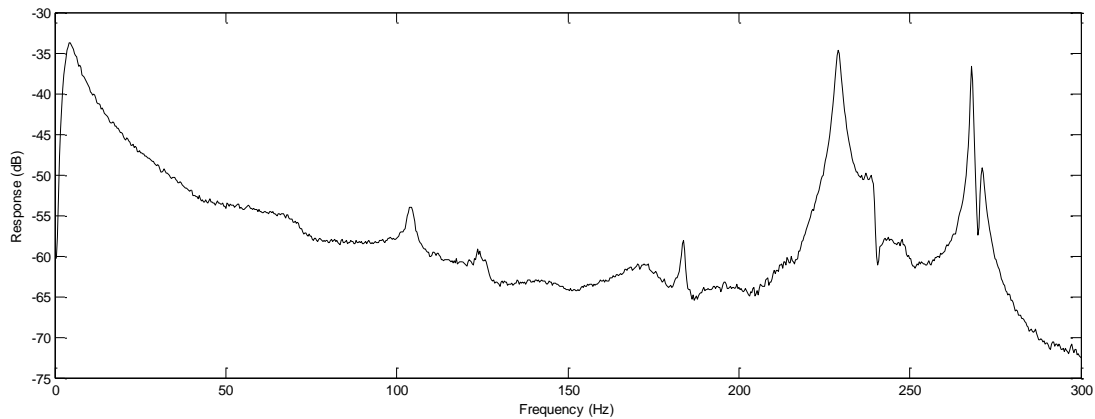


Figure 4.9. Averaged Fourier transform across a side plate.

It's immediately apparent that the side plate of the vibrating structure has two minor modes at 104 and 183 Hz and two main modes at 229 and 268 Hz. The large tapering peak at low frequencies does not represent a vibrational mode but is merely the rigid body motion of the structure moving with the shake table. Figure 4.10 shows a displacement representation of the modes each of these four frequencies. Mode A at 104 Hz shows the two top corners of the side plate vibrating opposite each other. Mode B at 183 Hz shows the center of plate as well as the top edge vibrating with each other. Mode C at 229 Hz shows only the center of the plate vibrating. Mode D at 268 Hz shows the center of the plate and the top edge vibrating opposite each other. The first two modes are so minor, however, that the first real mode that should be considered is mode C.

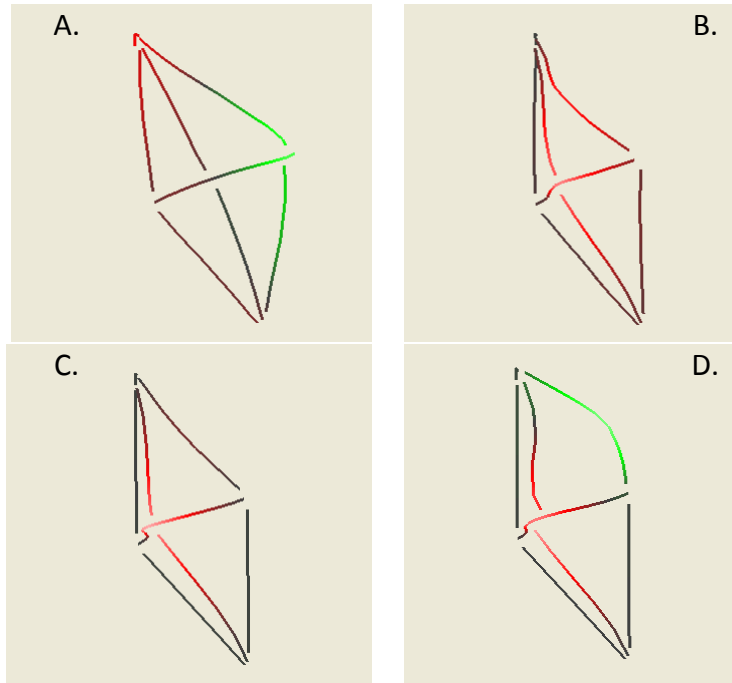


Figure 4.10. Vibrational modes of the side plate.

For the second data run, the structure was clocked 45 degrees on the shake table. This placed it with one of its corners facing forward. Due to the fact that the satellite corners overhang the Lightband, the satellite has the freedom to rock on the Lightband along its diagonal. Clocking the structure by 45 degrees aligns the diagonal with the horizontal excitation from the shake table to induce some amount of vertical excitation in the structure. The laser was repositioned above the structure looking down on its top. The final setup is shown in Figure 4.11 while the resulting averaged Fourier transform is plotted in Figure 4.12.



Figure 4.11. Setup for the second test.

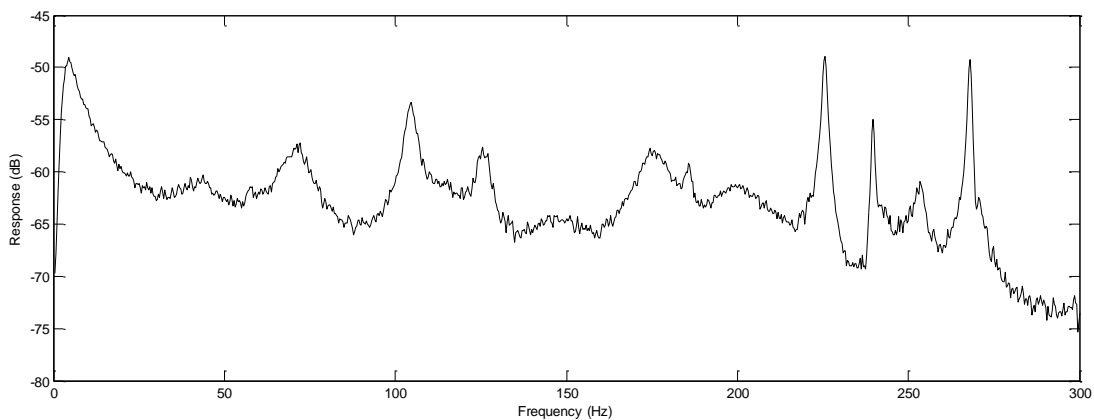


Figure 4.12. Averaged Fourier transform across the top plate.

When this test was begun, it was unclear how useful the resulting data would be considering the nonideal setup. It's very apparent how much less clean and coherent the data is in this second run compared to the data from the first run but it still proved quite useful. Two rough modes can be seen at 105 and 126 Hz while two much more well defined modes can be seen at 225 and 268 Hz. The displacement representation of the modes at these four frequencies can be seen in Figure 4.13. Mode E at 105 Hz shows each of the four corners of the structure vibrating with their opposite corner and opposite their neighboring corners. Mode F at 126 Hz shows the satellite roughly rocking on its diagonal. This is a vibrational mode that was expected to be captured with this setup. Mode G at 225 Hz shows two neighboring top edges vibrating with each other and opposite the other two edges. Mode H at 268 Hz simply shows two of the

top edges vibrating opposite each other. Ultimately, while these results were not ideal they were still useful.

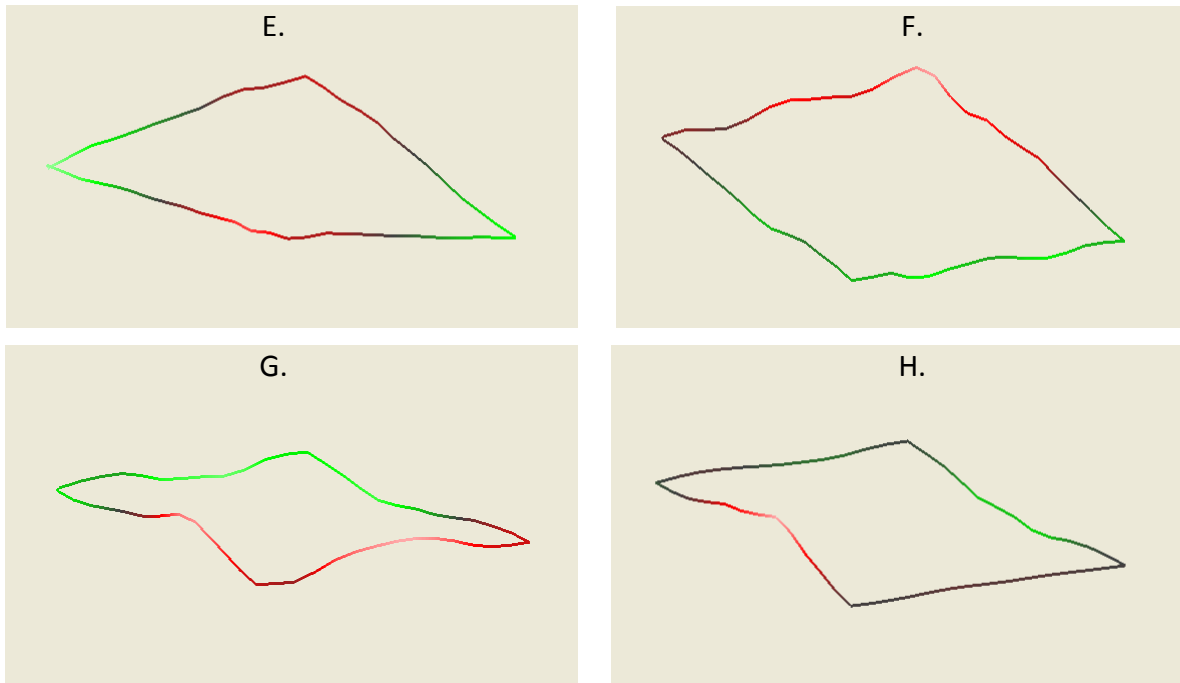


Figure 4.13. Vibrational modes of the top plate.

In general, both tests produced modes that were expected to have some of the lowest frequencies so they correlated quite well with an intuitive understanding of the structure. More importantly, all of the modes found in these tests were above the 100 Hz requirement and all of the main modes were well above 200 Hz.

Table 5.1 Lowest 10 modes of FEA test structure

Frequency	Mode (testing correspondence)
281	Rocking mode along diagonal. (F)
288	Rocking mode along other diagonal. (F)
302	Horizontal Vibration of corners. (A)
307	Vertical vibration of structure corners. (E)
353	Squashing of structure.
390	Vibration on interior of side plates. (C)
393	Vibration on interior of side plates. (C)
411	Vibration of side plates.
470	Interior side plates opposite their top edge. (D)
488	Interior side plates opposite their top edge. (D)

It's great to see how many of the lowest frequency modes given by the FEA correspond directly to modes that came up in the testing. Unfortunately, none of the corresponding modes actually match their testing counterparts. In fact, the frequencies given by the FEA are all at least 100 Hz higher than those found through testing. It's difficult to say what exactly is causing such a wide disparity. Probably the most significant contributor is the nonideal nature of the test structure. From edges that don't all perfectly align to bolts that don't perfectly bind, all of these things allow some leeway for the structure to vibrate more freely and reduce the overall natural frequencies. For lack of a stronger correlation, a very rough first-order rule of thumb we can use moving forward is that the actual frequency for a particular vibrational mode will be about 150 Hz less than that given by the FEA.

Packing Structure Model and Analysis

Now that it's clear how the testing results and the FEA results compare, it's possible to move on to a more complex model with a base reference. As an intermediate step, just the newly designed structure was considered. Again, the part files were imported from the 3D CAD software to Abaqus, assembled, and constrained to each other as shown in Figure 5.2. The ten lowest frequency modes of the structure are tabulated below.

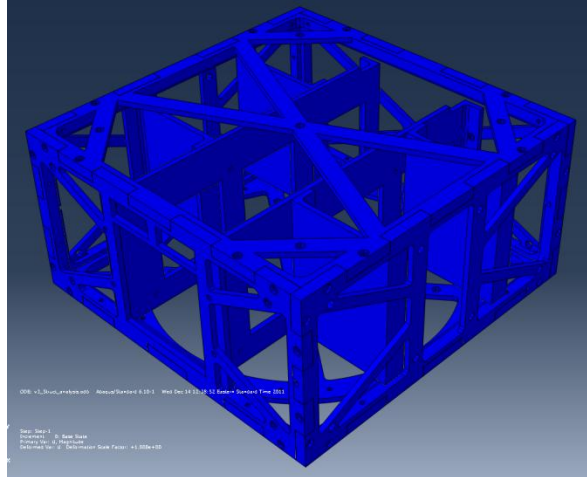


Figure 5.2. Completed Abaqus model of the redesigned structure.

Table 5.2 Lowest 10 modes of FEA redesigned structure

Frequency	Mode
298	Vibration of top crosspiece.
373	Vibration of bottom crosspiece.
522	Rocking along diagonal.
532	Uncertain.
606	Vertical vibration of unconstrained top edge.
734	Horizontal vibration of right and left halves opposite each other.
801	Secondary mode of top crosspiece.
845	Horizontal vibration of front and back halves.
921	Horizontal vibration of top crosspiece and unconstrained edge.
982	Twisting vibration of top crosspiece.

Unsurprisingly, all that additional internal supporting structure helps to really constrain everything and increase the frequencies as a result. The two lowest frequencies result from the vibration of the two largest unconstrained pieces of the structure. Indeed, multiple of the listed modes are the result of the top crosspiece being unconstrained at its center. Attaching it to the internal supports in some way would be a quick and easy solution. All of the modes except for the first one or two are well outside the region where they would warrant more detailed examination.

Such a rigid structure is a good starting point for analyzing the packing model. Using the previous model as a base, part models for several of the larger and heavier components including the PPOD, thrusters, and battery box were imported to Abaqus. They were constrained to the various plates as closely as possible to how they would actually be attached.

All component parts were assumed to be rigid bodies. Smaller components were grouped as point masses and attached to the various plates. The final FEA model for the packed satellite is shown in Figure 5.3 below and the lowest ten frequency modes are listed in Table 5.3.

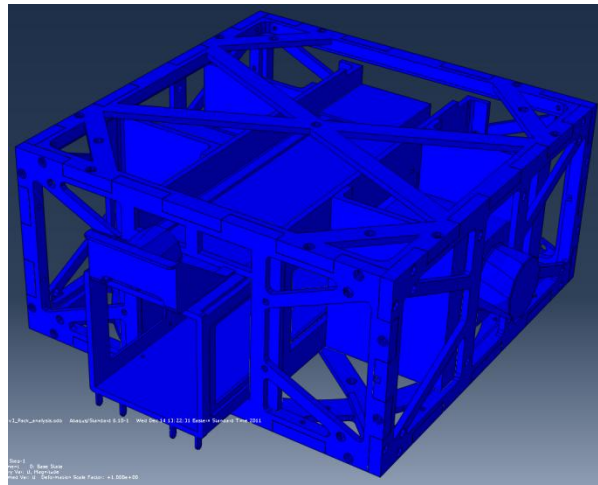


Figure 5.3. Completed Abaqus model of the redesigned packing.

Table 5.3 Lowest 10 modes of FEA redesigned packing

Frequency	Mode
301	Vibration of top crosspiece.
374	Vibration of bottom crosspiece.
494	Horizontal vibration of right thruster.
496	Horizontal vibration of left thruster.
527	Vertical vibration of right thruster.
590	Vertical vibration of unconstrained top edge.
614	Vertical vibration of left thruster.
637	Twisting vibration of left and right halves
722	Uncertain.
807	Secondary mode of the top crosspiece.

There's a good correlation between the structural modes that carried over from the last list, primarily those with the top and bottom crosspieces. Various vibrational modes of the two thrusters show up throughout the list. This is due to the fact that the thrusters attach at their very front but their actual center of mass sits much farther back allowing them to oscillate about their attachment points like a pendulum. Moving the smaller internal support plates closer to the thrusters would increase the frequency of these oscillations substantially. Of course, these modes don't seem to be in any danger of failing the 100 Hz requirement as they currently are.

Overall, the redesigned structure and packing seem to be in very good position to meet the UNP structural requirements. Of course, physical testing is needed to be certain but it'd be difficult to believe that some of these modes would drop many hundreds of Hertz in frequency in the translation from ideal model to fabricated structure.

VI. CONCLUSION

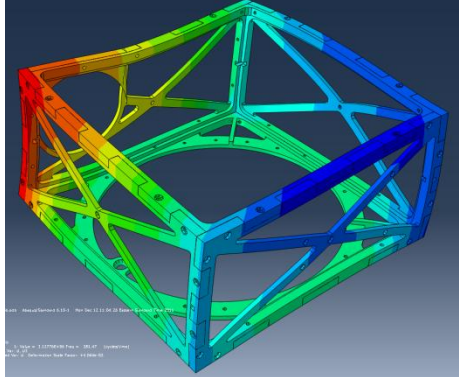
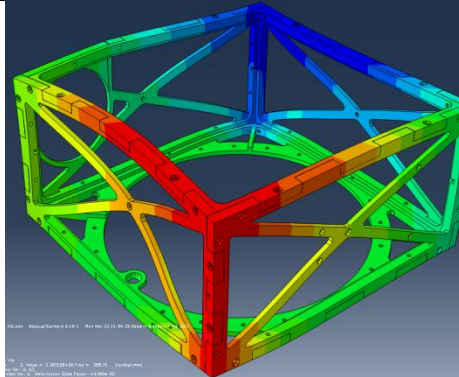
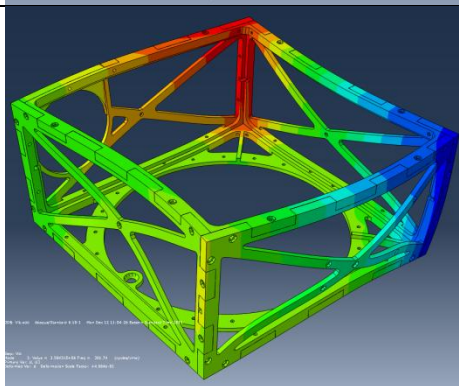
The correlation between the physical testing results and the FEA results was unable to be achieved to the extent required. However, the FEA results did successfully predict which vibrational modes would have the lowest frequency. The frequency offset between these corresponding modes was in the range of 100-200 Hz. It's difficult to say why the frequencies dropped so sharply from the FEA model to the test structure but the culprit is most likely the imperfections introduced when machining an actual structure as compared to the ideal edges and constraints of the FEA model. The testing confirmed that the structure alone passed UNP requirements.

If the first order rule of thumb is used and the frequencies gained from the FEA of the redesigned structure and packing are reduced by ~150 Hz it's clear that they would meet the requirements as well. There are one or two area with frequencies that place them low enough to warrant a second look (primarily the top crosspiece) but these have relatively simple design solutions that wouldn't impact the rest of the structure. Even still, it should be a priority to work toward machining and testing the new structure to be sure.

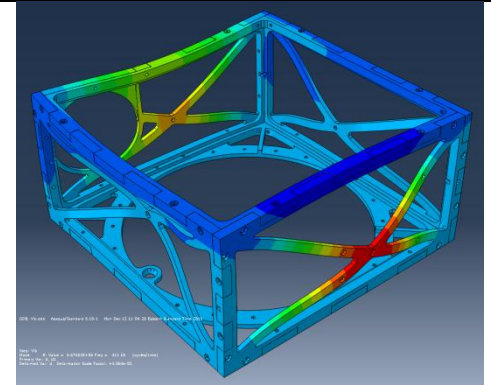
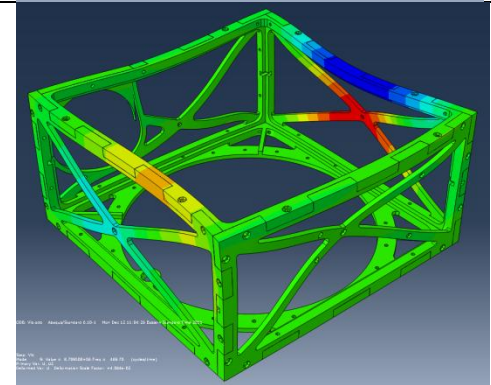
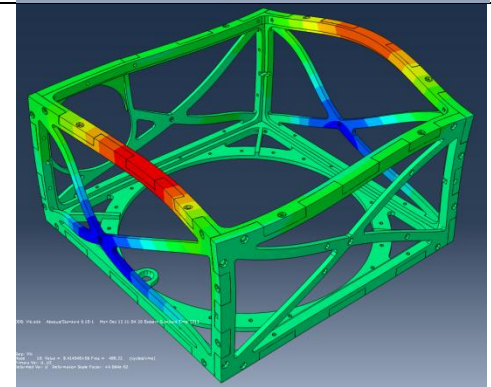
This project began with goals of designing a structure that was smaller, lighter, better able to meet UNP requirements, and easier and more reliable to machine. By those standards this structural design developed for has been demonstrated to succeed admirably.

**APPENDIX A:
Images of Vibrational Modes from Analysis**

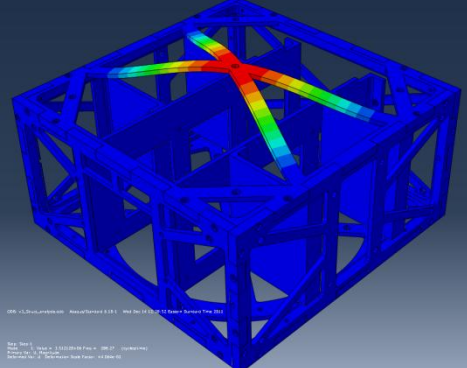
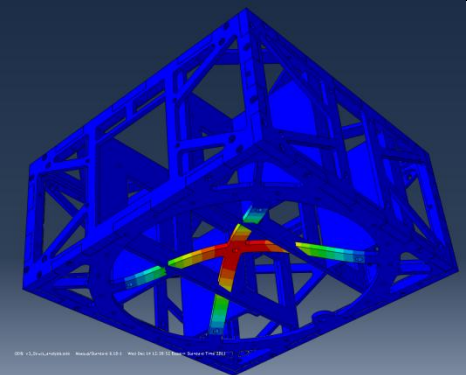
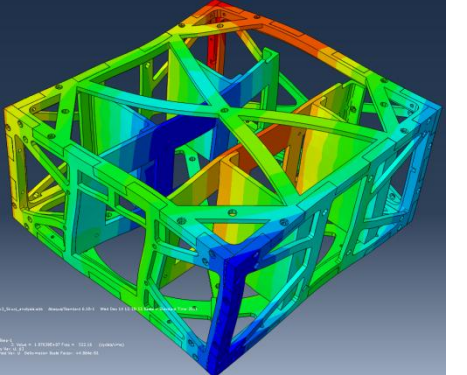
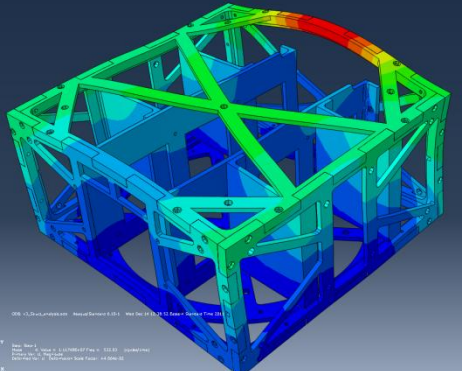
1. Test Structure

Displacement Representation	Frequency	Mode
	281	Rocking mode along diagonal. (F)
	288	Rocking mode along other diagonal. (F)
	302	Horizontal Vibration of corners. (A)

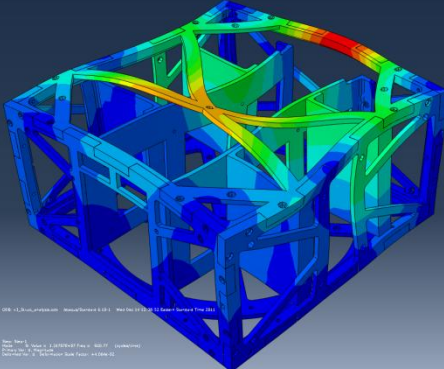
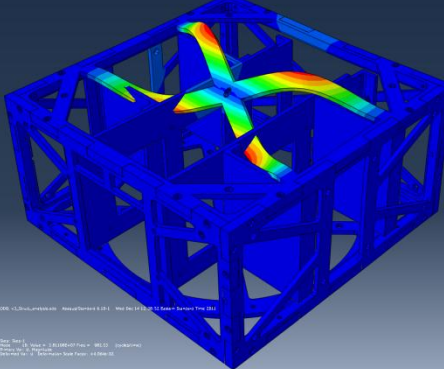
	<p>307</p>	<p>Vertical vibration of structure corners. (E)</p>
	<p>353</p>	<p>Squashing of structure.</p>
	<p>390</p>	<p>Vibration on interior of side plates. (C)</p>
	<p>393</p>	<p>Vibration on interior of side plates. (C)</p>

	<p>411</p>	<p>Vibration of side plates.</p>
	<p>470</p>	<p>Interior side plates opposite their top edge. (D)</p>
	<p>488</p>	<p>Interior side plates opposite their top edge. (D)</p>

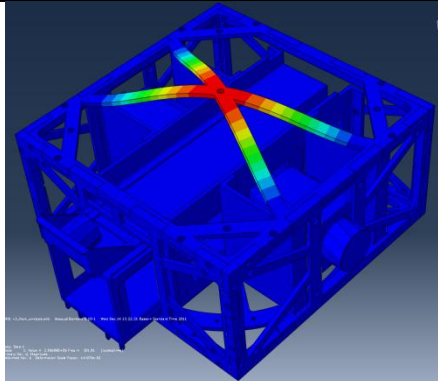
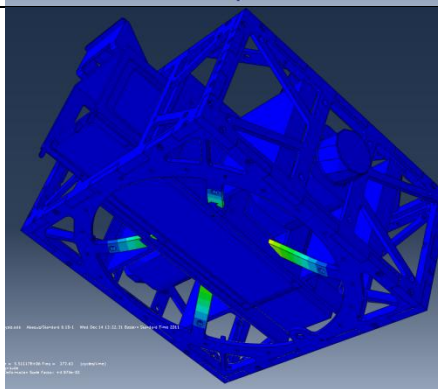
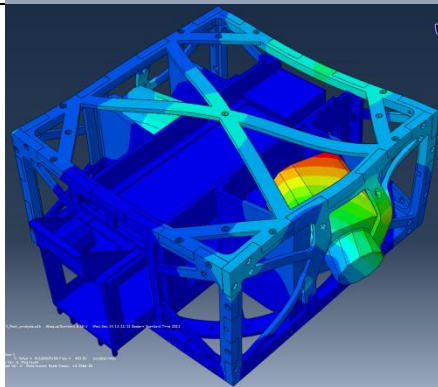
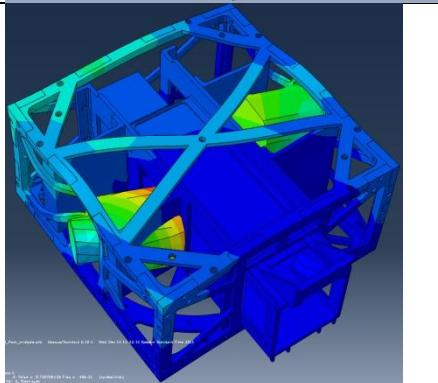
2. Redesigned Structure

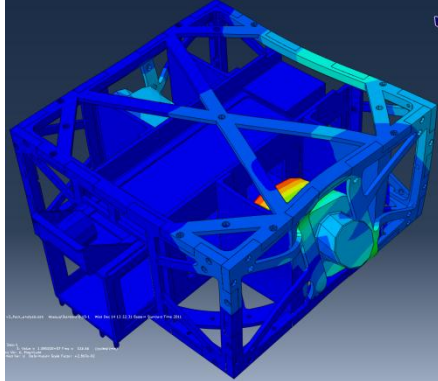
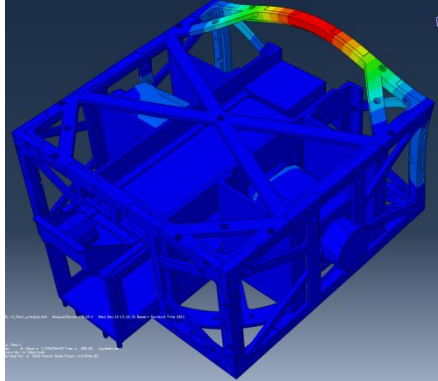
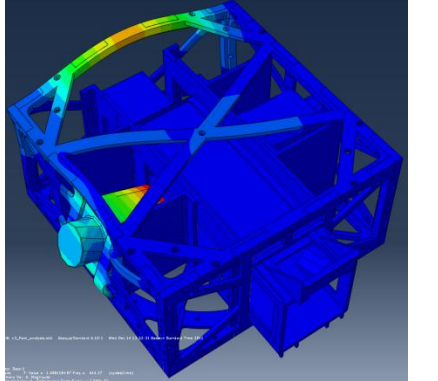
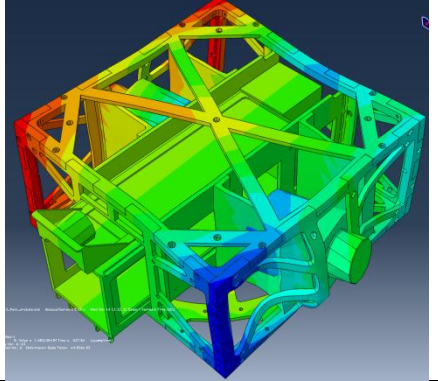
Displacement Representation	Frequency	Mode
	298	Vibration of top crosspiece.
	373	Vibration of bottom crosspiece.
	522	Rocking along diagonal.
	532	Uncertain.

	<p>606</p>	<p>Vertical vibration of unconstrained top edge.</p>
	<p>734</p>	<p>Horizontal vibration of right and left halves opposite each other.</p>
	<p>801</p>	<p>Secondary mode of top crosspiece.</p>
	<p>845</p>	<p>Horizontal vibration of front and back halves.</p>

	<p>921</p>	<p>Horizontal vibration of top crosspiece and unconstrained edge.</p>
	<p>982</p>	<p>Twisting vibration of top crosspiece.</p>

3. Redesigned Packing

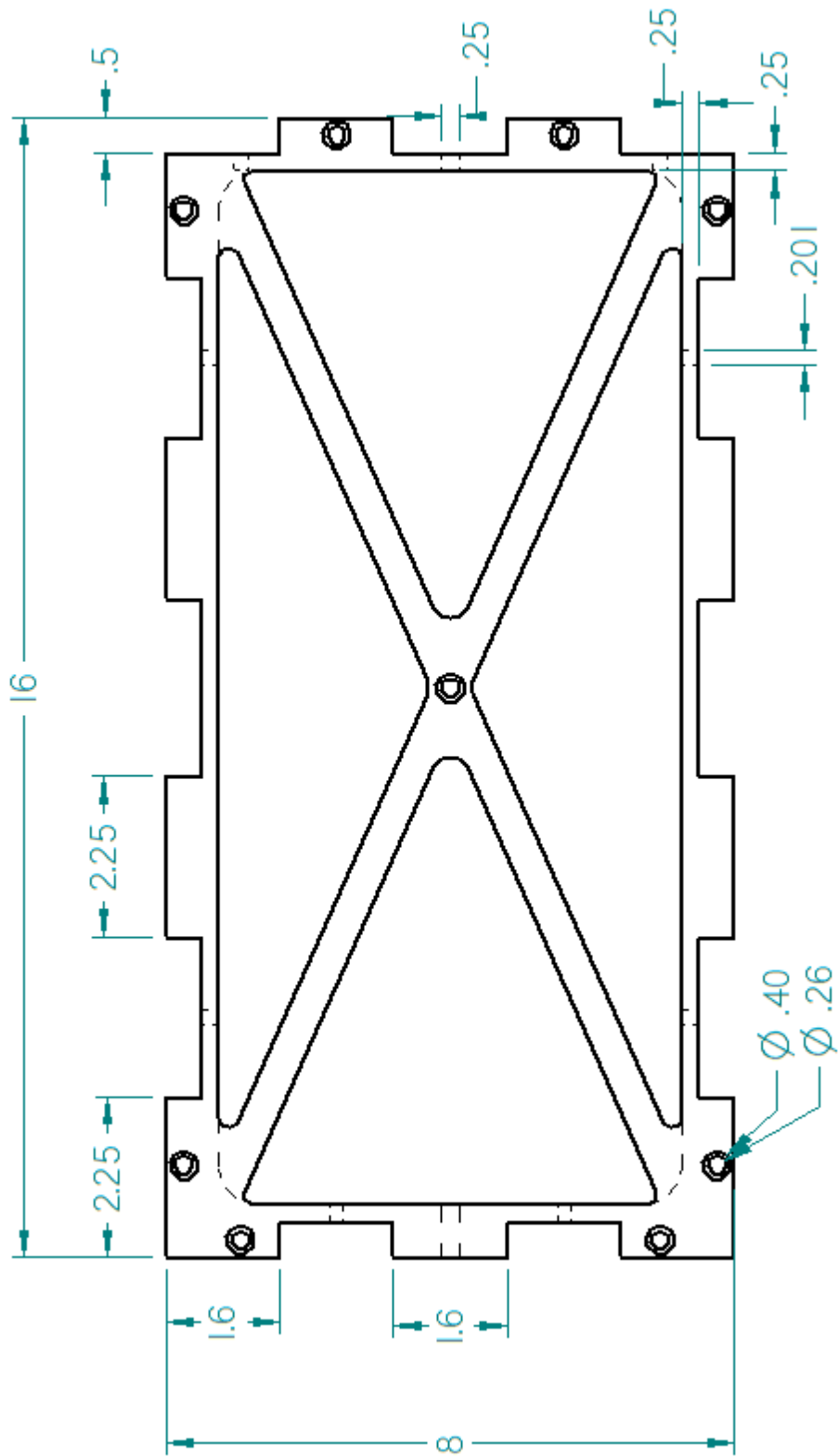
Displacement Representation	Frequency	Mode
	301	Vibration of top crosspiece.
	374	Vibration of bottom crosspiece.
	494	Horizontal vibration of right thruster.
	496	Horizontal vibration of left thruster.

	527	Vertical vibration of right thruster.
	590	Vertical vibration of unconstrained top edge.
	614	Vertical vibration of left thruster.
	637	Twisting vibration of left and right halves

	<p>722</p>	<p>Uncertain.</p>
	<p>807</p>	<p>Secondary mode of the top crosspiece.</p>

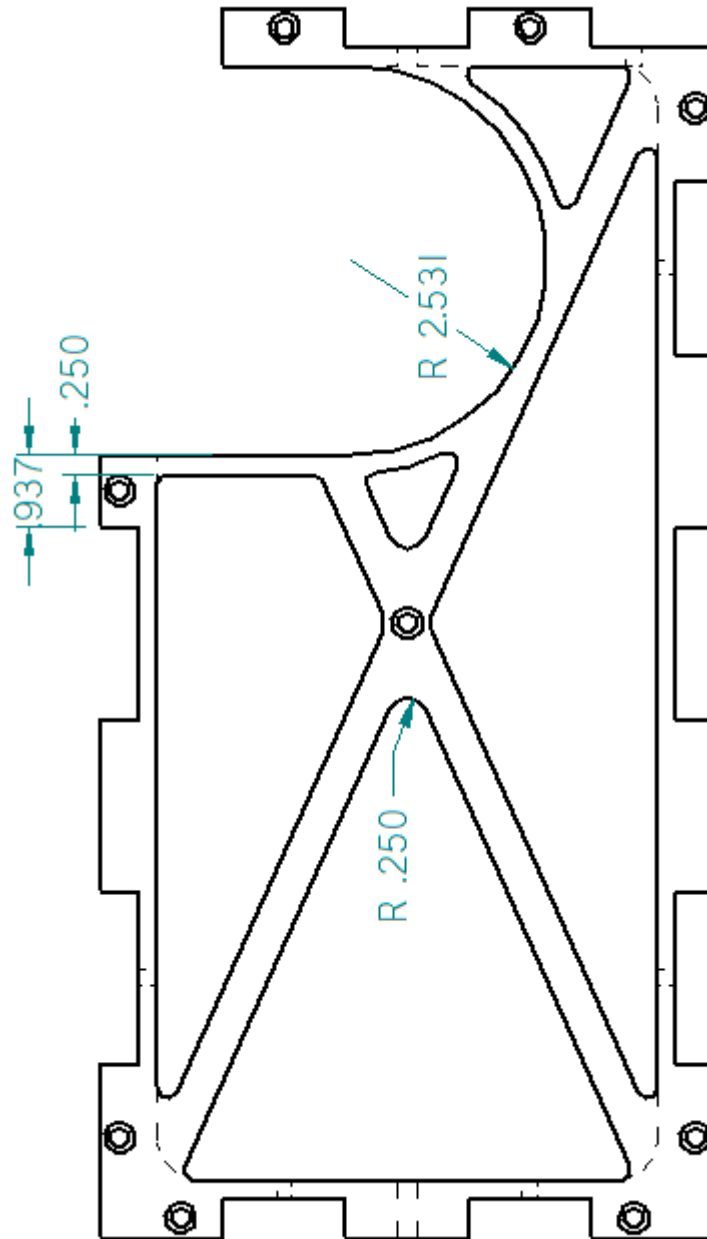
APPENDIX B:
Part Drawings for the Test Structure and Interface
(All dimensions in inches)

Side Plate

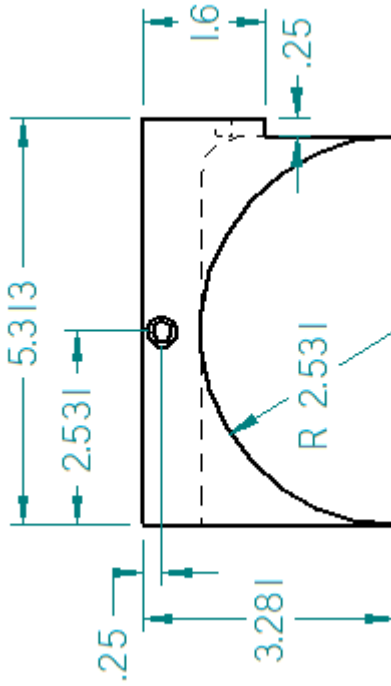


Side Plate with Star Tracker Cutout

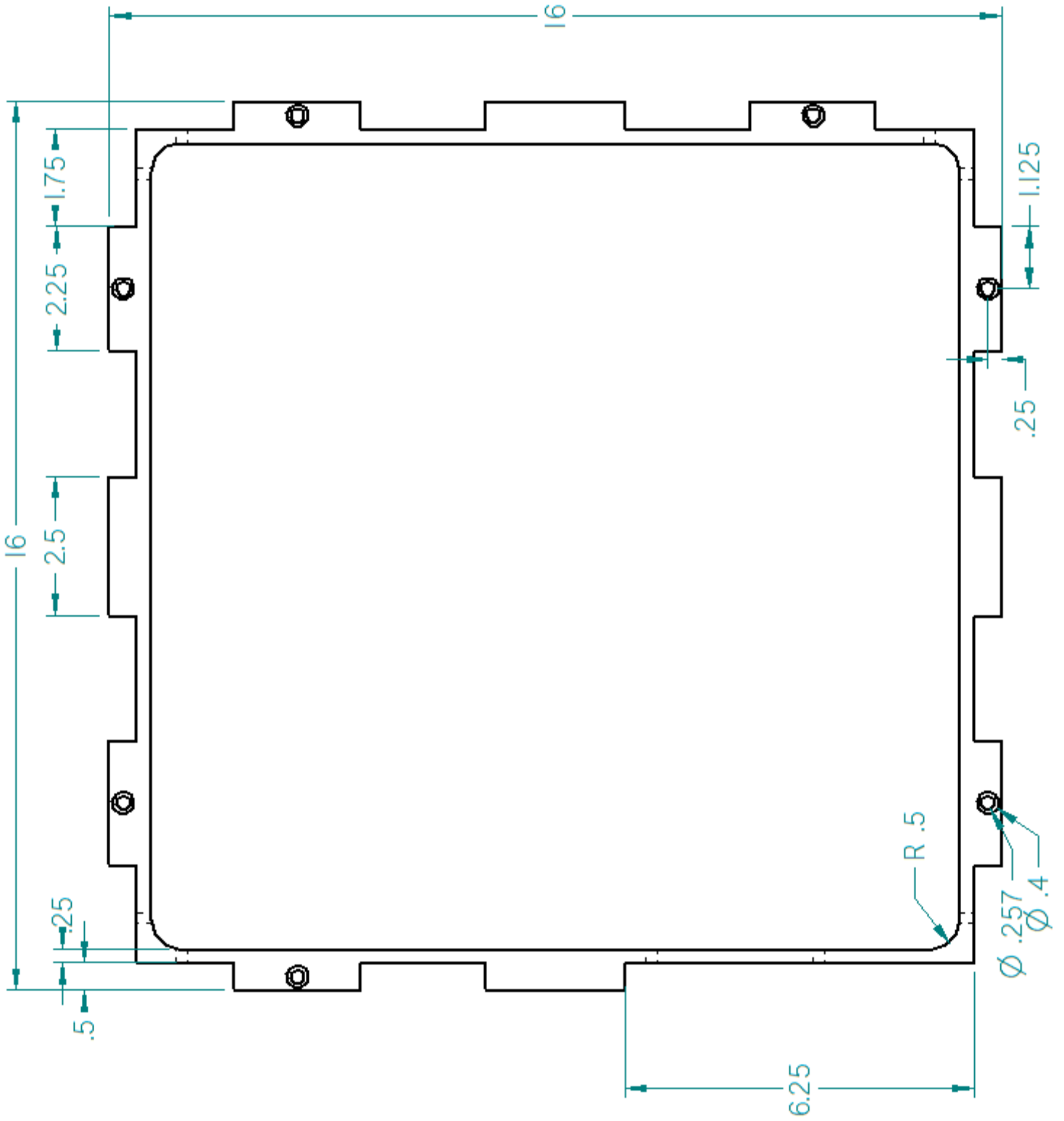
(Dimensions same as Side Plate unless otherwise noted)



Star Tracker Plate



Top Plate



LVI Plate

(Dimensions same as Top Plate unless otherwise noted)

